Electronic Supplementary Material (ESI) for Environmental Science: Nano.

Supplementary file

Characterization of aerosolized particles from nanoclay-enabled composites during manipulation processes

Eun Gyung Lee, Lorenzo Cena, Jiwoon Kwon, Ali Afshari, HaeDong Park, Gary Casuccio, Kristin Bunker, Traci Lersch, Ashley Gall, Huy Pham, Alixandra Wagner, Sushant Agarwal, Cerasela Zoica Dinu, Rakesh Gupta, Sherri Friend, Todd A. Stueckle

Supplemental Method

A. Generation of nano-enabled composite materials

Nanoclay-enabled composite blocks were prepared in a two-step process. First, PP resin was mixed with a Cloisite nanoclay by melt mixing in a Thermo-Haake internal mixer. Melt mixing is a widely used method to produce nanoclay composites usually resulting in a mixed morphology of exfoliated and intercalated nanoclay structures within the matrix. The temperatures, mixing times, and press times used during composite synthesis were highly consistent with the previous studies (Mazrouaa 2012; Alateyah et al. 2013; Muller et al. 2017). PP pellets were placed in the mixer rotating at 80 rpm and allowed to melt for 1 minute at 180 °C. The Cloisite (either 93A or 25A) was then added to the melted PP and mixed for 4 minutes. In the second step, the composite mix was placed in a compression molding machine heated to 204 °C lined with aluminum foil. After letting the material melt for 5 minutes, the plates of the molding machine were closed at 5 tons of pressure for 5 minutes. The molds were then removed and allowed to cool at room temperature. The data indicated the presence of both exfoliated nanoclay platelets and intercalated structures within the nanocomposite. Based on our detailed analysis of the nanocomposite, the degree of exfoliation between each nanoclay's coating type and the % load was adequate for this study and is representative of ONC-enabled PP composites currently in use.

References:

A. M. Mazrouaa, chapter 14 - Polypropylene nanocomposites, in “Polypropylene”, Edited Fatih
Dogan, InTech, Croatia (2012) 265-286.

Alateyah AI, Dhakal HN, Zhang ZY. Processing, properties, and applications of polymer nanocomposites based on layered silicates: a review. Adv Polymer Technol. 2013, 32(4), 21368.

Muller K, Bugnicourt E, Latorre, M, Jorda M, Sanz, YE, et al. Review on the processing and properties of polymer nanocomposites and nanocoatings and their applications in the packaging, automotive, and energy fields. Nanomaterials 2017, 7,74.

B. Characterization of mechanical properties

For each composite material (virgin PP and all nanoclay-enabled composites), mechanical properties including Young's modulus, tensile strength, toughness, and elongation at break were determined as previously described in Wagner et al.[42] Briefly, rectangular sections measuring 32.5 mm long x 5.5 mm wide x 3.2 mm thick were cut and subjected to testing on an Instron E1000 (Instrom Corporation, Norwood, MA) under a 2 kN load cell operated by Bluehill 3 software (Instrom Corporation). For this purpose, each section was placed in grips and tested under crosshead speed of 5 mm/min. Toughness was then calculated by integrating the area under stress by strain curve.

Crystallinity of each composite was determined with a PANalytical X'Pert Pro XRD (Malvern PANalytical, Royston, UK) using a Cu-kα1 8047.2 eV source at 45 kV and 40 mA with a 10 sec/step in the 5-90° 2θ range. Prior to the analysis, the samples were cut into squares, mounted onto the instrument's spinner stage, and evaluated using a 15 mm beam mask size.

The degree of dispersion of nanoclay within the PP matrix was evaluated with a Bruker D8 Discovery X-ray Diffractometer (XRD) (Bruker, Madison, WI) by determining exfoliation (i.e., the separation distance between the embedded nanoclay platelets). Samples were mounted onto the sample holder via double-sided tape and the Bruker was aligned. Diffraction was obtained using a Cu-kα1 8047.2 eV source operating at 40 kV and 40 mA with scan speed of 10 sec/step in the 1-10° 2θ range at increments of 0.02°. The peak location was determined using an optical spectroscopy software (Spectragryph v1.2.10, Oberstdorf, Germany). Detailed information for the method is in Wagner et al.[42]

Visualization of dispersed nanoclay within the PP matrix of each composite material was performed via a transmission electron microscopy (TEM) analysis. Briefly, nanocomposite shavings removed from the composite's leading edge were cut into 1 mm strips and placed in 4 ml vials of epoxy resin (LX-112 embedding kit, Ladd Research Inc., Williston, VT) on a rotary mixer. The samples were exchanged into fresh resin each day for 3 days to allow the resin to infiltrate into the nanocomposite. At the end of day 3, each individual strip of nanocomposite was embedded into a capsule of fresh resin and polymerized for 48 hours in a 60 °C oven. The resulting block was sectioned at 70 nm thickness, placed on a TEM grid, and examined using JEOL 1400 TEM (Model 1400, JEOL Inc., Tokyo, Japan) at 80 kV.

C. Criteria applied to establish particle classification

During the CCSEM/EDS analysis, the energy and abundance of X-rays emitted by a particle were displayed as spectrum of X-ray counts verses energy, and the X-ray counts for each element were determined by the processing of the spectrum. The individual particles of the CCSEM data were classified into particle types according to their elemental composition. This was accomplished using a set of rules developed through examination of the EDS results obtained from the composite and sandpaper samples. For a particle to be classified to a specific particle type, it must conform to the elemental criteria listed in Table S1. In this table, elemental criteria are defined for thirteen particle types. Each individual particle was tested against these rules in succession beginning with the first type until the conditions of a class were satisfied. If a particle did not fall into one of the predefined particle types, it was classified in the miscellaneous category. The classification of composite particles is described in the electron microscopy analysis section.

Supplemental Tables

Table S1. Criteria applied to establish CCSEM particle classification rules

Particle Class	Elemental Criteria
Composite	C+O>80% - Plus manual evaluation of trace elements and morphology
Na-F-Al	Na>=10% and F>=10% and Al>3%
Si-Ca	Si>20% and Ca>10% and Si+Ca+O+C>50%
Si-Al	Si>20% and Al>5% and Si+Al+O+C>50%
Si-rich	Si>30% and C+Si+O>70%
Ca-rich	Ca>20% and C+Ca+O>70%
Al-Zr	Al>10% and Zr>10%
Zr-rich	Zr>30%
Al-rich	Al>20% and Al+O+C>50% and Si<10%
Fe-rich	Fe>=15% and Fe+C+O>50%
C(NaF)	C+O>60% and Na>1% and F>1%
C-rich	C+O>80%
Misc.	All remaining particles

Table S2. Summary of particle number concentrations using silicon carbide sandpaper.

Material ID	Composites	Sandpaper grit	Average number concentration (particles cm^{-3})
PP	Polypropylene (PP) (virgin)	P120	31213
		P320	6549
1%25A-PP	Cloisite 25A-PP (1% w/w)	P120	48809
		P320	NC
4%25A-PP	Cloisite 25A-PP (4% w/w)	P120	27038
		P320	NC
1%93A-PP	Cloisite 93A-PP (1% w/w)	P120	29712
		P320	NC
4%93A-PP	Cloisite 93A-PP (4% w/w)	P120	35870
		P320	NC

NC: Test not conducted

Table S3. Temperatures measured at the surface where a composite block contacted the sandpaper

Material ID	Sandpaper grit	Before sanding (°C)	9-min sanding (°C)	22-min sanding (°C)	Δ (22-min – before) (°C)
PP	P100	23.0	28.1	28.2	5.2
	P180	24.8	28.1	28.7	3.9
1%25A-PP	P100	25.7	30.2	31.1	5.4
	P180	24.1	28.2	29.7	5.5
4%25A-PP	P100	24.9	29.9	30.9	6.0
	P180	23.7	28.4	29.6	5.9
1%93A-PP	P100	24.0	29.6	30.6	6.7
	P180	24.5	28.6	29.8	5.2
4%93A-PP	P100	25.0	30.5	31.7	6.8
	P180	24.9	30.4	31.7	6.7

Note that the temperatures were measured during the sample collection with various direct-reading instruments. No temperatures were measured during the stabilization of particle concentrations in the chamber.

Table S4. Average elemental compositions for each composite dust sample based on relative X-ray counts for each particle class. Each column in the table pertains to the relative percentage of X-ray counts of each element averaged for each particle assigned to the class. The last line provides the overall average X-ray counts attributed to all particle classes considered together normalized to 100 percent.

- Average composition for particle classes on sample 1%25A-PP (P100, IOM filter)

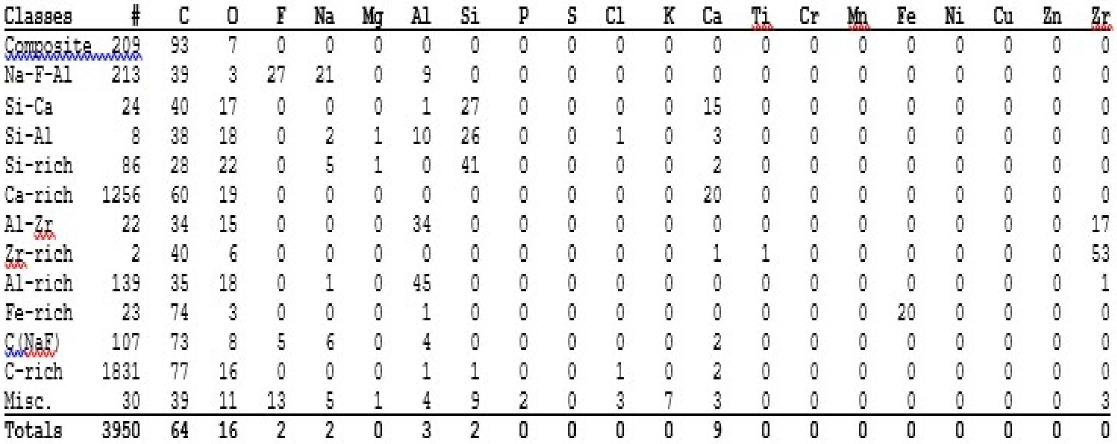

Classes	#	C	O	F	Na	Mg	Al	Si	P	S	Cl	K	Ca	Ti	Cr	Mn	Fe	Ni	Cu	Zn	Zr
Composite	209	93	7	0	0	0	0	0	0	0	0	0	0	0	0	0	0	0	0	0	0
Na-F-Al	213	39	3	27	21	0	9	0	0	0	0	0	0	0	0	0	0	0	0	0	0
Si-Ca	24	40	17	0	0	0	1	27	0	0	0	0	15	0	0	0	0	0	0	0	0
Si-Al	8	38	18	0	2	1	10	26	0	0	1	0	3	0	0	0	0	0	0	0	0
Si-rich	86	28	22	0	5	1	0	41	0	0	0	0	2	0	0	0	0	0	0	0	0
Ca-rich	1256	60	19	0	0	0	0	0	0	0	0	0	20	0	0	0	0	0	0	0	0
Al-Zr	22	34	15	0	0	0	34	0	0	0	0	0	0	0	0	0	0	0	0	0	17
Zr-rich	2	40	6	0	0	0	0	0	0	0	0	0	1	1	0	0	0	0	0	0	53
Al-rich	139	35	18	0	1	0	45	0	0	0	0	0	0	0	0	0	0	0	0	0	1
Fe-rich	23	74	3	0	0	0	1	0	0	0	0	0	0	0	0	0	20	0	0	0	0
C(NaF)	107	73	8	5	6	0	4	0	0	0	0	0	2	0	0	0	0	0	0	0	0
C-rich	1831	77	16	0	0	0	1	1	0	0	1	0	2	0	0	0	0	0	0	0	0
Misc.	30	39	11	13	5	1	4	9	2	0	3	7	3	0	0	0	0	0	0	0	3
Totals	3950	64	16	2	2	0	3	2	0	0	0	0	9	0	0	0	0	0	0	0	0

- Average composition for particle classes on sample 4%25A-PP (P100, IOM filter)

- Average composition for particle classes on sample 1%93A-PP (P100, IOM filter)

- Average composition for particle classes on sample 4%93A-PP (P100, IOM filter)

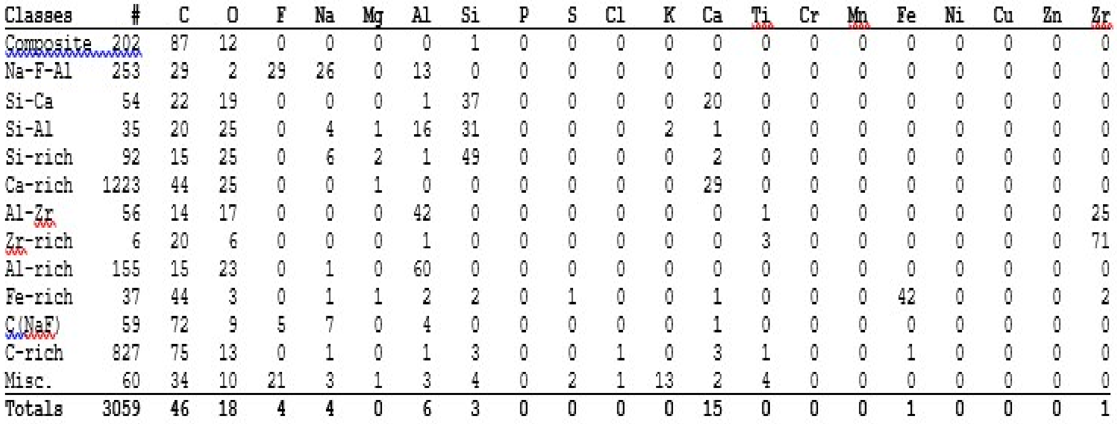

Classes	#	C	O	F	Na	Mg	Al	Si	P	S	Cl	K	Ca	Ti	Cr	Mn	Fe	Ni	Cu	Zn	Zr
Composite	202	87	12	0	0	0	0	1	0	0	0	0	0	0	0	0	0	0	0	0	0
Na-F-Al	253	29	2	29	26	0	13	0	0	0	0	0	0	0	0	0	0	0	0	0	0
Si-Ca	54	22	19	0	0	0	1	37	0	0	0	0	20	0	0	0	0	0	0	0	0
Si-Al	35	20	25	0	4	1	16	31	0	0	0	2	1	0	0	0	0	0	0	0	0
Si-rich	92	15	25	0	6	2	1	49	0	0	0	0	2	0	0	0	0	0	0	0	0
Ca-rich	1223	44	25	0	0	1	0	0	0	0	0	0	29	0	0	0	0	0	0	0	0
Al-Zr	56	14	17	0	0	0	42	0	0	0	0	0	0	1	0	0	0	0	0	0	25
Zr-rich	6	20	6	0	0	0	1	0	0	0	0	0	0	3	0	0	0	0	0	0	71
Al-rich	155	15	23	0	1	0	60	0	0	0	0	0	0	0	0	0	0	0	0	0	0
Fe-rich	37	44	3	0	1	1	2	2	0	1	0	0	1	0	0	0	42	0	0	0	2
C(NaF)	59	72	9	5	7	0	4	0	0	0	0	0	1	0	0	0	0	0	0	0	0
C-rich	827	75	13	0	1	0	1	3	0	0	1	0	3	1	0	0	1	0	0	0	0
Misc.	60	34	10	21	3	1	3	4	0	2	1	13	2	4	0	0	0	0	0	0	0
Totals	3059	46	18	4	4	0	6	3	0	0	0	0	15	0	0	0	1	0	0	0	1

- Average composition for particle classes on sample Sandpaper only (Bulk)

Supplemental Figures

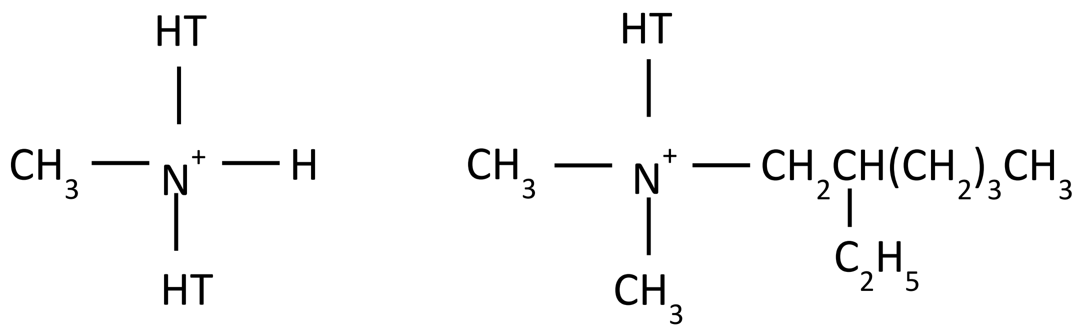
$$CH_3-\overset{HT}{\underset{HT}{N^+}}-H$$

$$CH_3-\overset{HT}{\underset{CH_3}{N^+}}-CH_2\underset{C_2H_5}{CH}(CH_2)_3CH_3$$

Cloisite 93A **Cloisite 25A**

Fig. S1. Chemical structures of Cloisite 25A® and Cloisite 93A®. HT indicates dehydrogenated tallow.

A

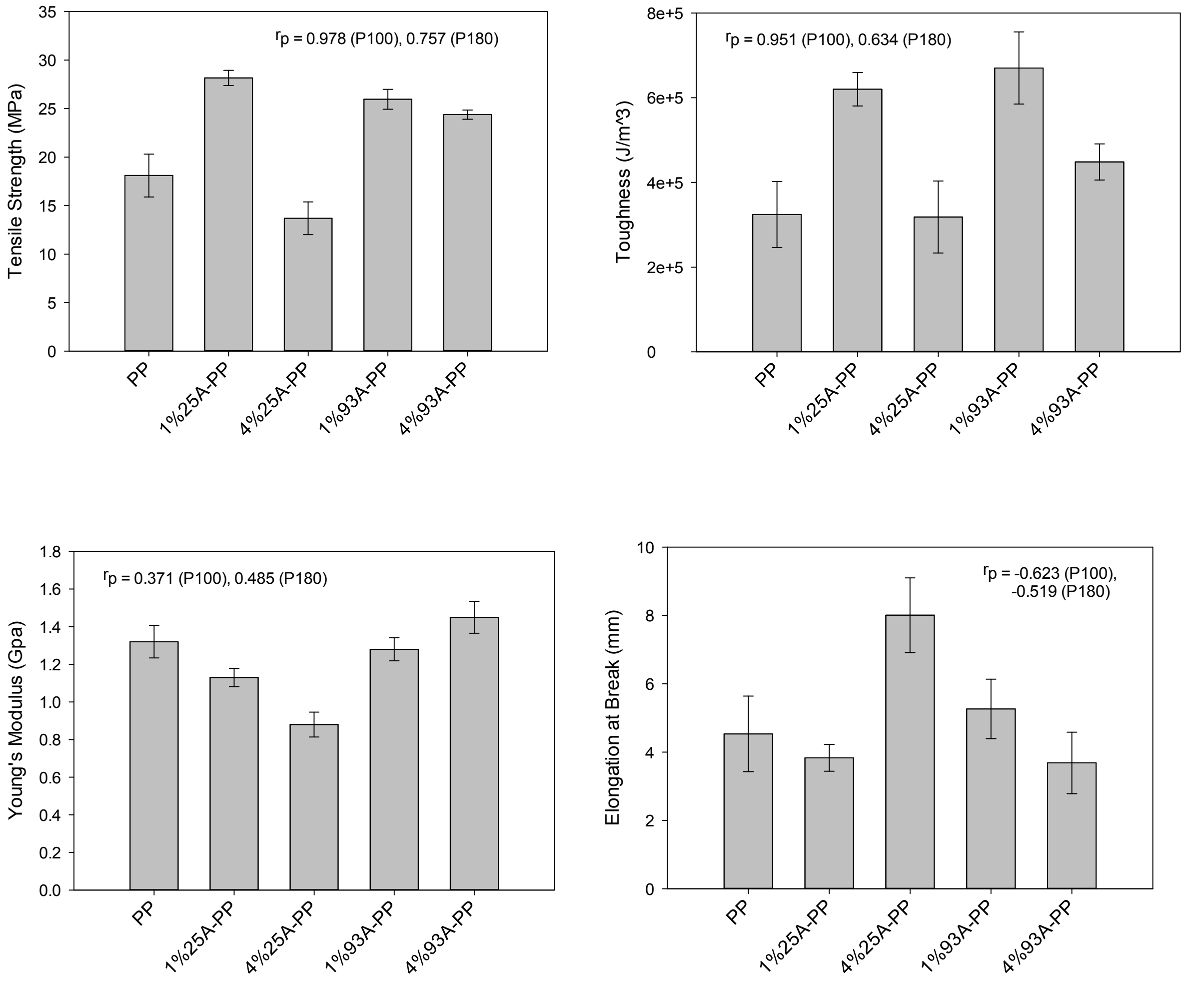
Tensile Strength (MPa)
0
5
10
15
20
25
30
35
ʳp = 0.978 (P100), 0.757 (P180)
PP
1%25A-PP
4%25A-PP
1%93A-PP
4%93A-PP
Toughness (J/m^3)
0
2e+5
4e+5
6e+5
8e+5
ʳp = 0.951 (P100), 0.634 (P180)
PP
1%25A-PP
4%25A-PP
1%93A-PP
4%93A-PP
Young's Modulus (Gpa)
0.0
0.2
0.4
0.6
0.8
1.0
1.2
1.4
1.6
1.8
ʳp = 0.371 (P100), 0.485 (P180)
PP
1%25A-PP
4%25A-PP
1%93A-PP
4%93A-PP
Elongation at Break (mm)
0
2
4
6
8
10
ʳp = -0.623 (P100),
-0.519 (P180)
PP
1%25A-PP
4%25A-PP
1%93A-PP
4%93A-PP

B

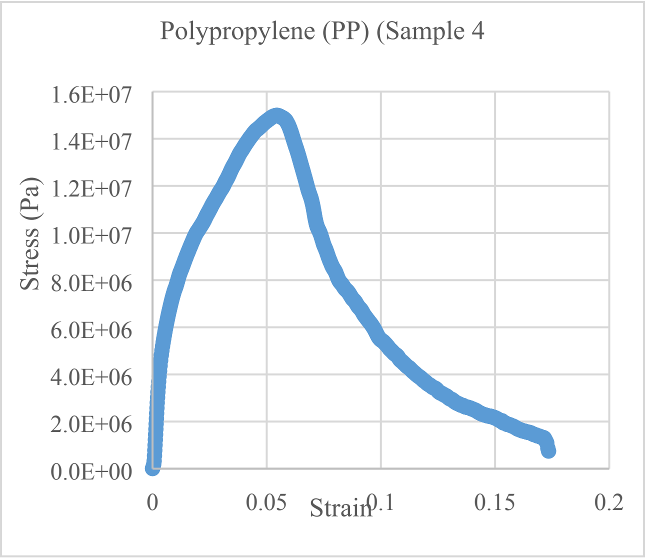
Polypropylene (PP) (Sample 4
Stress (Pa)
0.0E+00
2.0E+06
4.0E+06
6.0E+06
8.0E+06
1.0E+07
1.2E+07
1.4E+07
1.6E+07
Strain
0
0.05
0.1
0.15
0.2

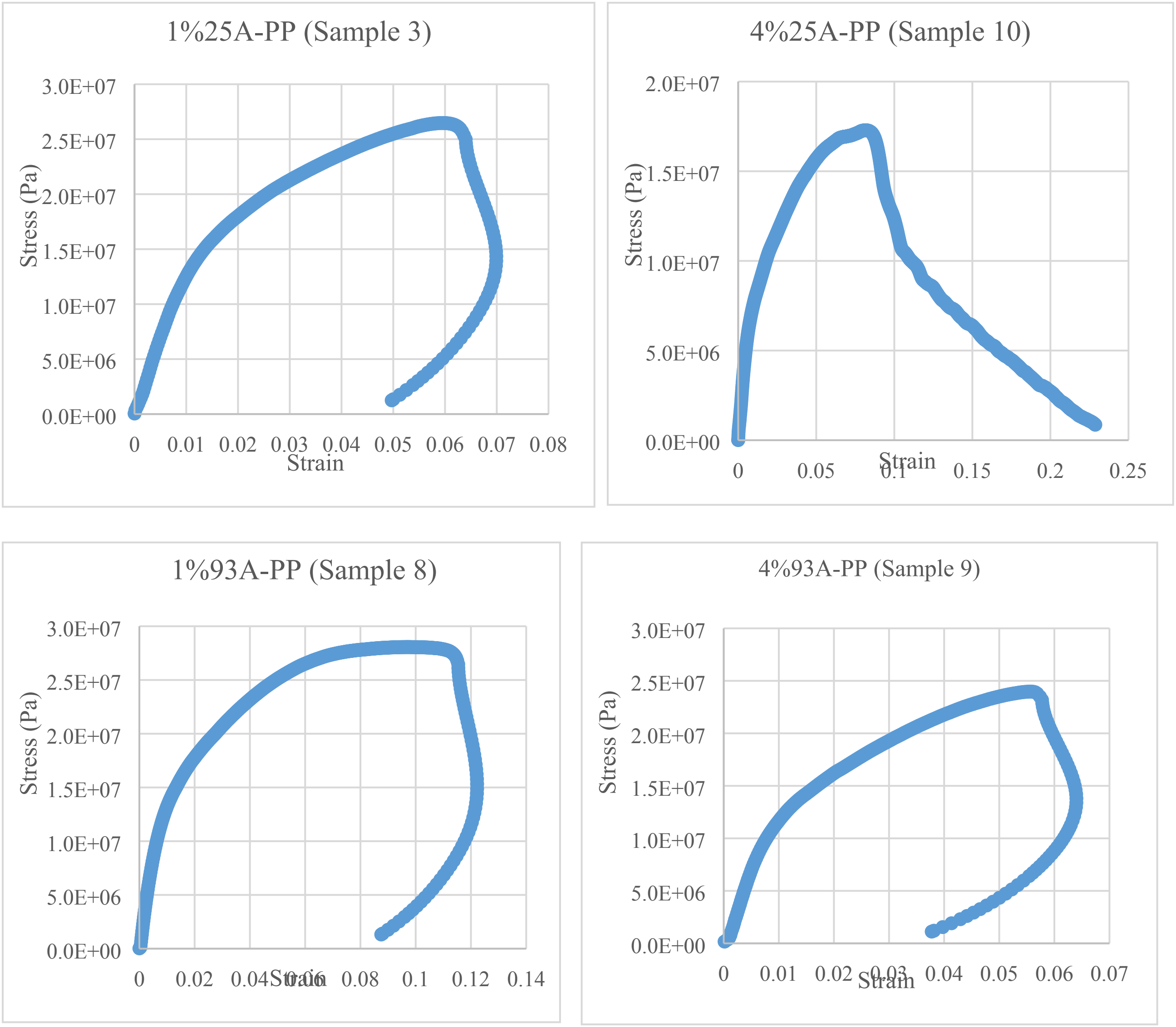

Fig. S2. Summary of mechanical properties of nanoclay-enabled polypropylene composites. A) Pearson correlation coefficient (r_p) indicates the relationship between the released particle number concentrations and individual mechanical properties. B) For each composite material, one out of 10 stress-strain curves were presented.

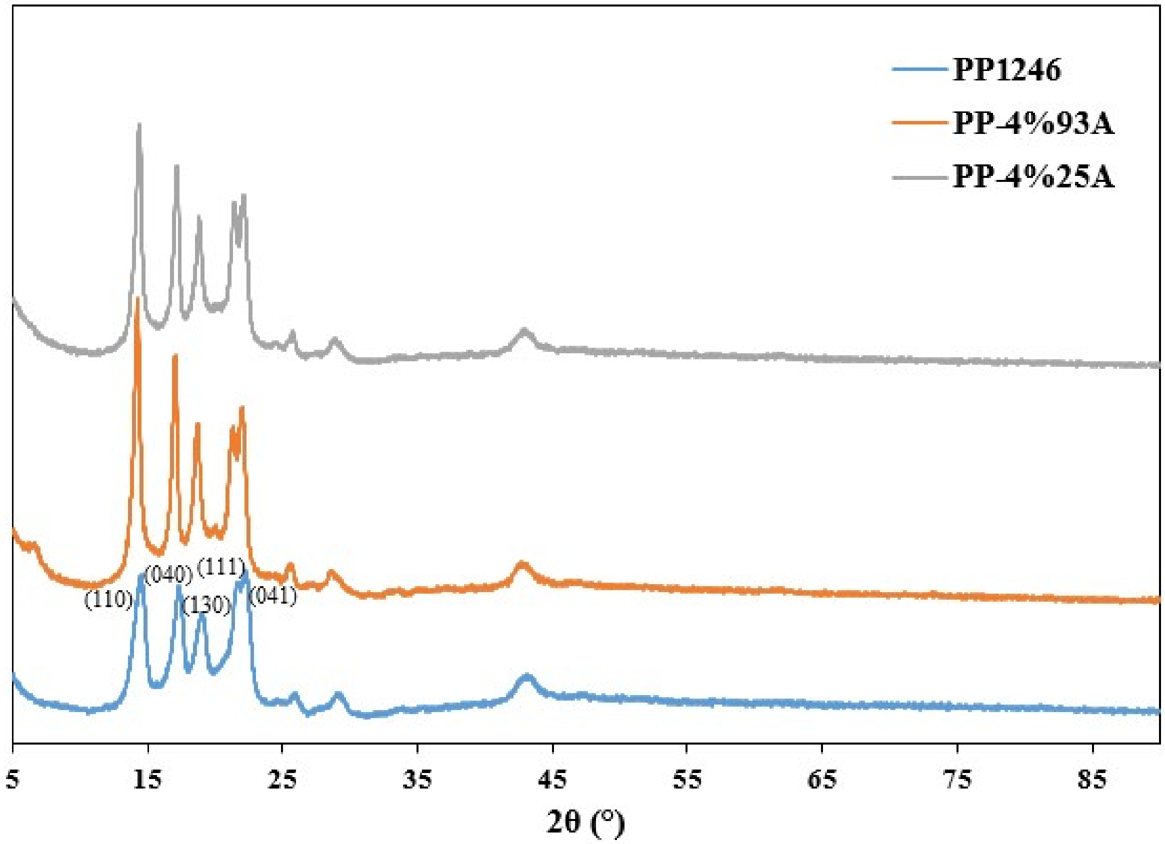

Fig. S3. Characteristic of crystallinity of nanoclay-enabled polypropylene composite compared to the virgin polypropylene (PP) determined by XRD. The diffraction peaks at the 2θ locations of 14.5, 17.4, 19.0, 21.8, and 22.3° correspond to the (110), (040), (130), (111), and (041) crystal planes.

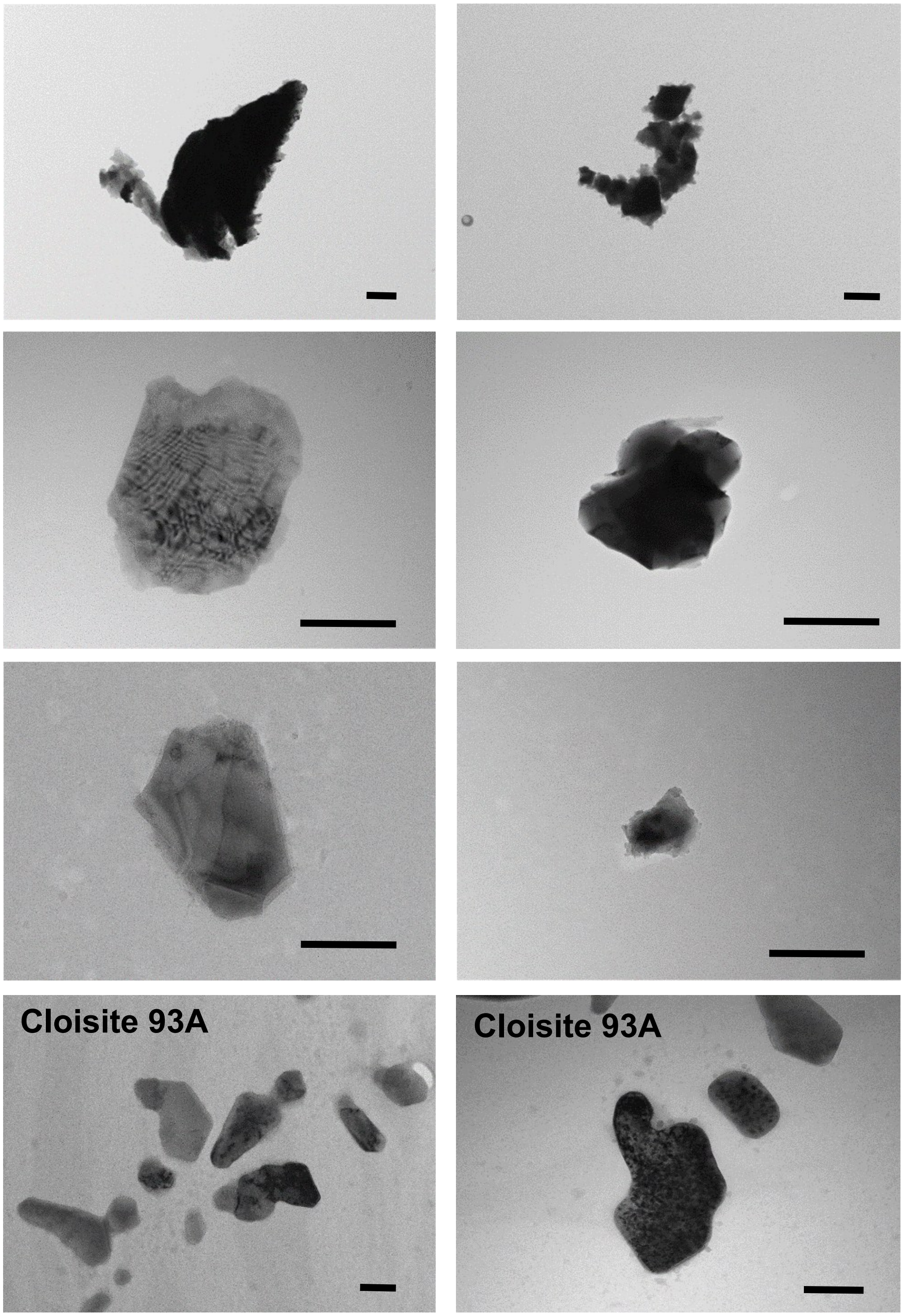

Fig. S4. Representative diversity of particulate collected on TEM grids during machining of 4% 93A PP nanocomposite via TEM analysis. As-prepared Cloisite 93A was imaged to assist in identifying free release of nanoclay. Scale bars represent 300 nm.

Sandpaper debris

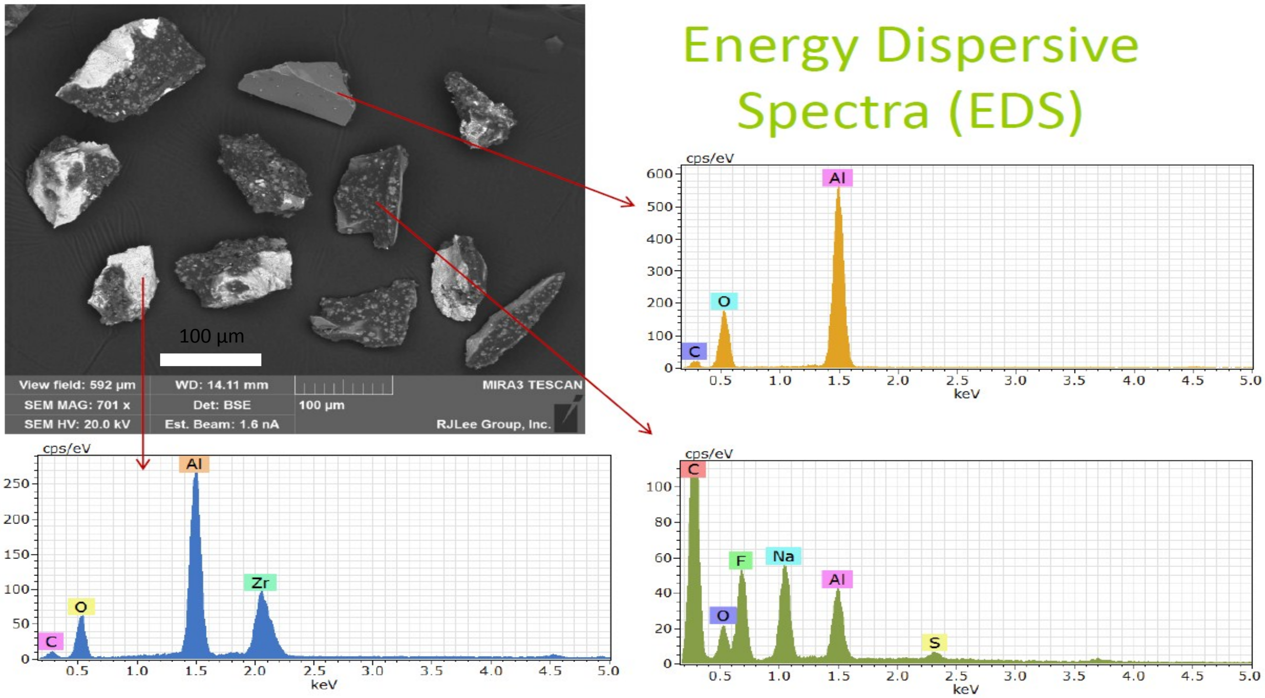

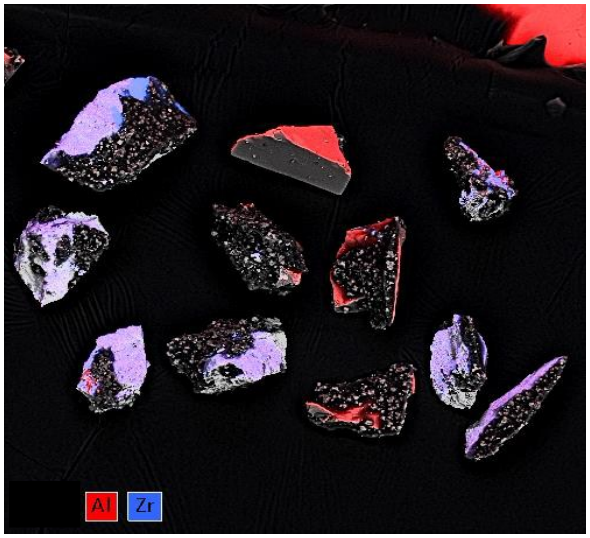

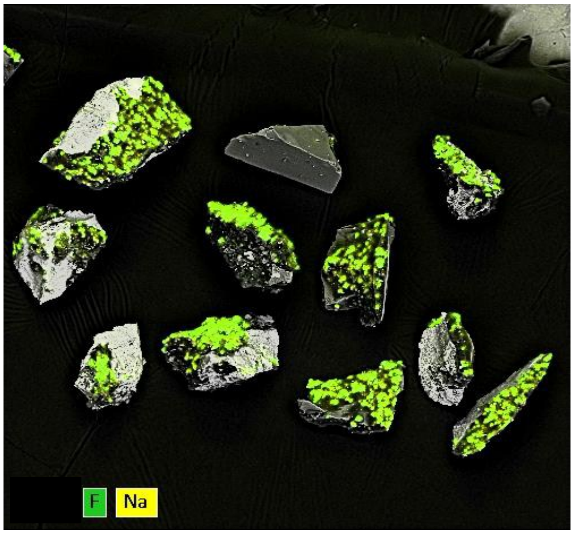

4%93A-PP

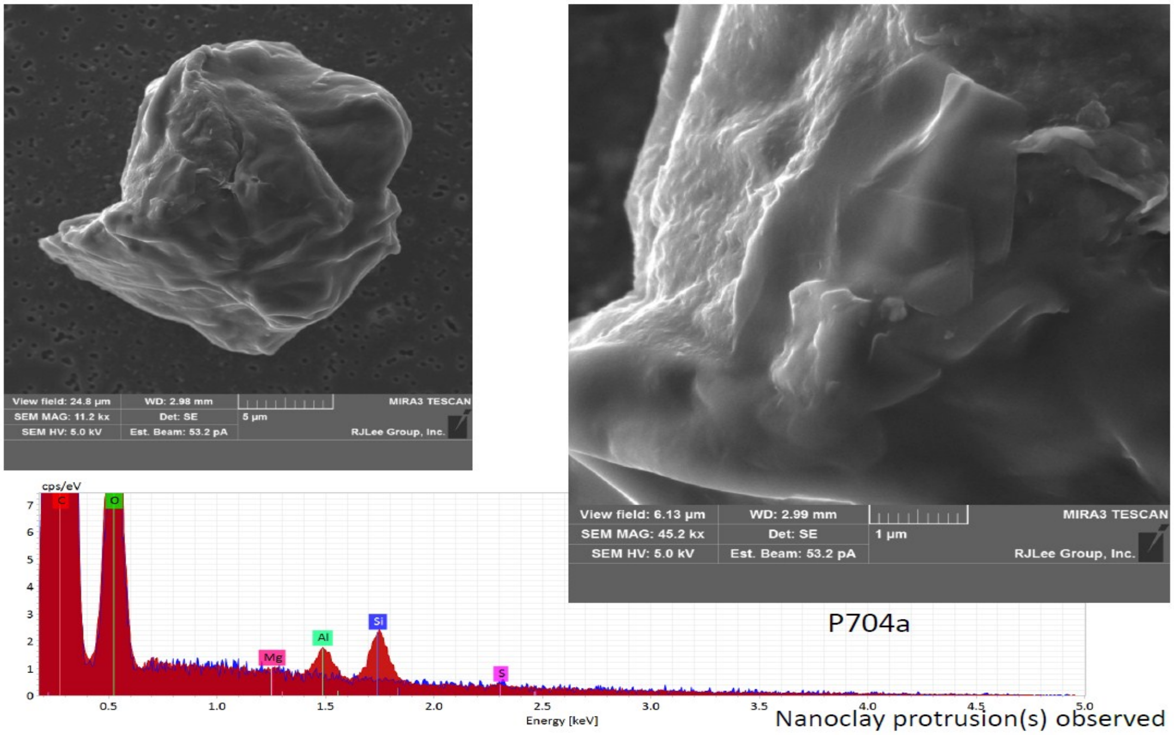

Nanoclay protrusion(s) observed

EDS overlay in blue was acquired from the particle; and the EDS in red was collected from the protrusion

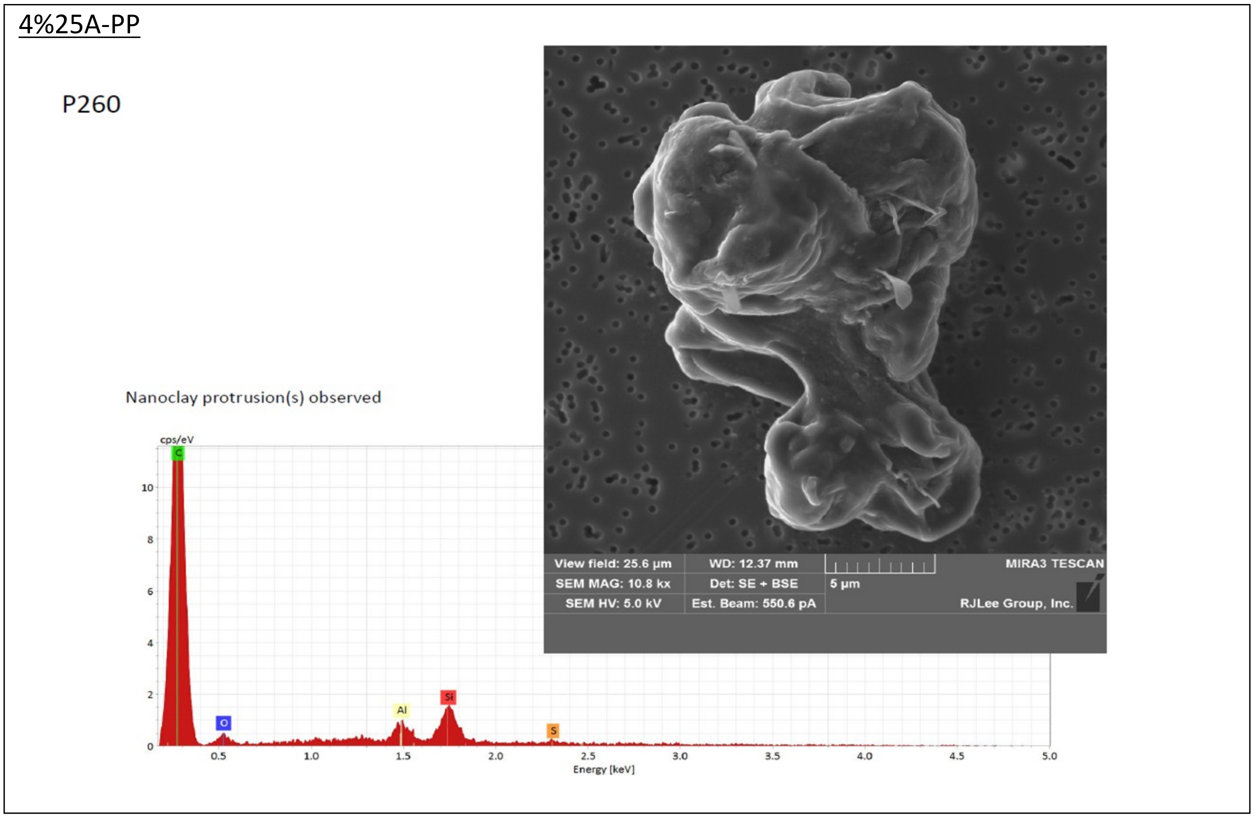

4%25A-PP

P260

Nanoclay protrusion(s) observed

Fig. S5. Morphology of sandpaper debris and composite particles

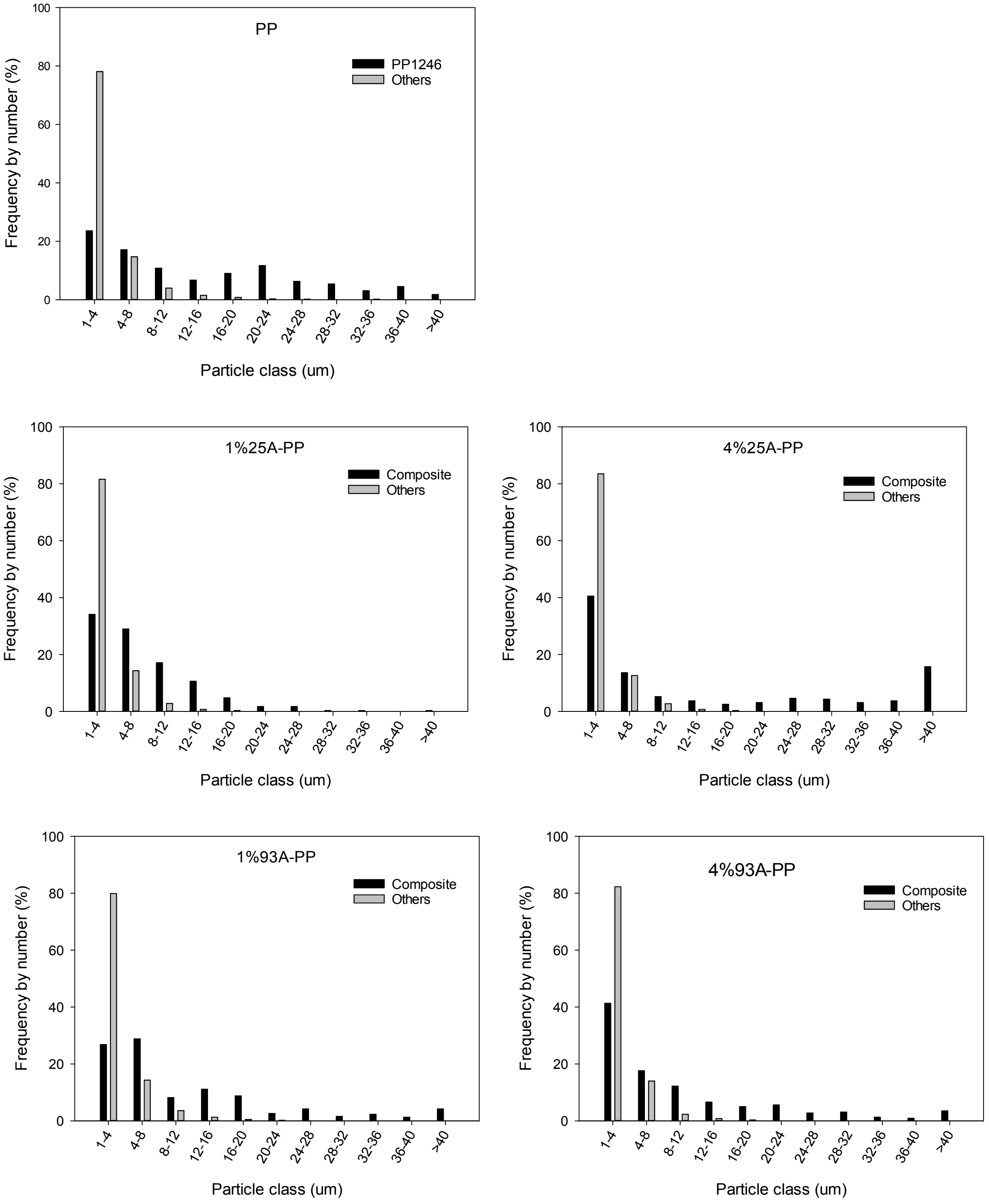

Fig. S6. Size distribution frequency by number (%) of nanoclay-enabled polypropylene composites.

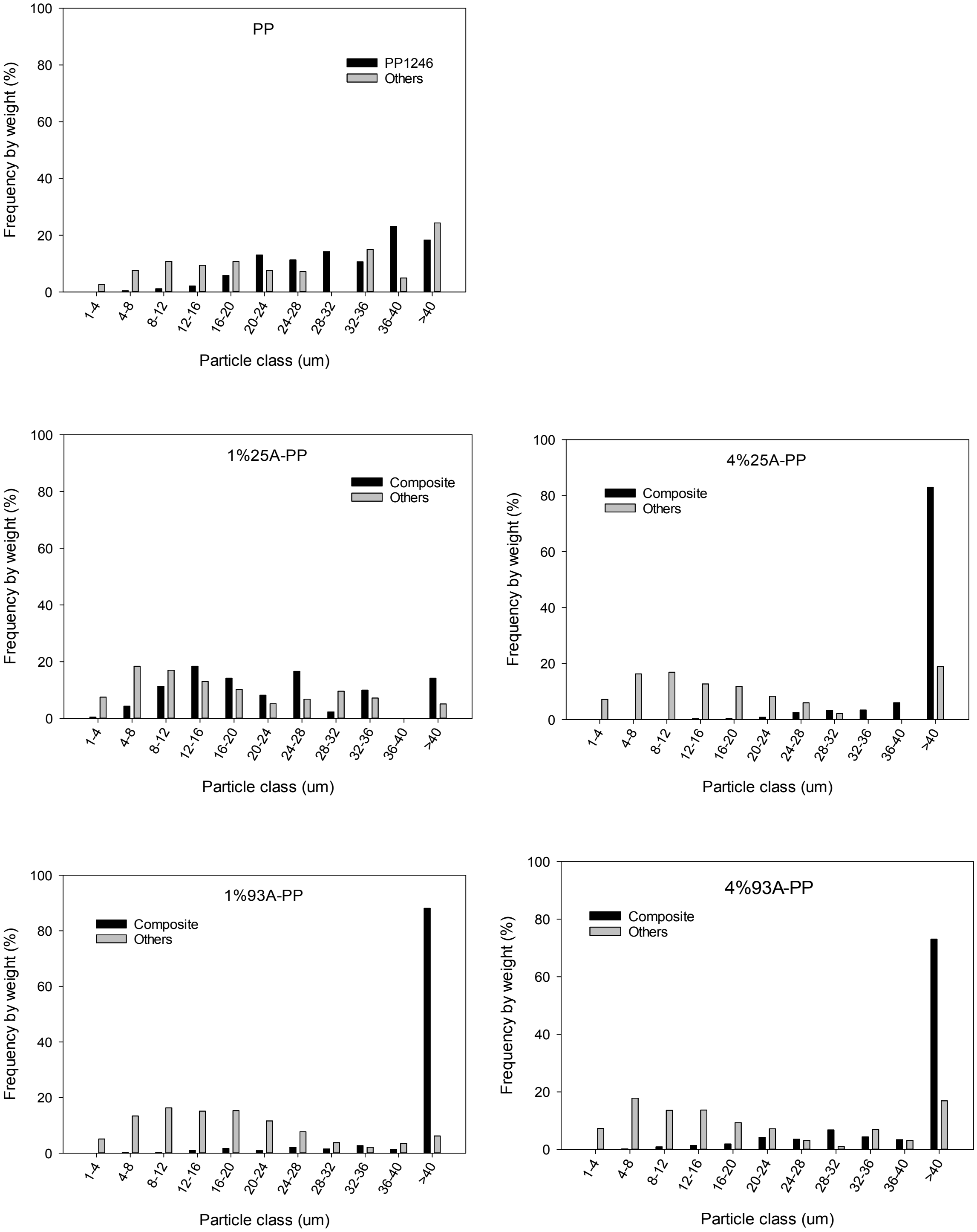

Fig. S7. Size distribution frequency by weight (%) of nanoclay-enabled polypropylene composites.

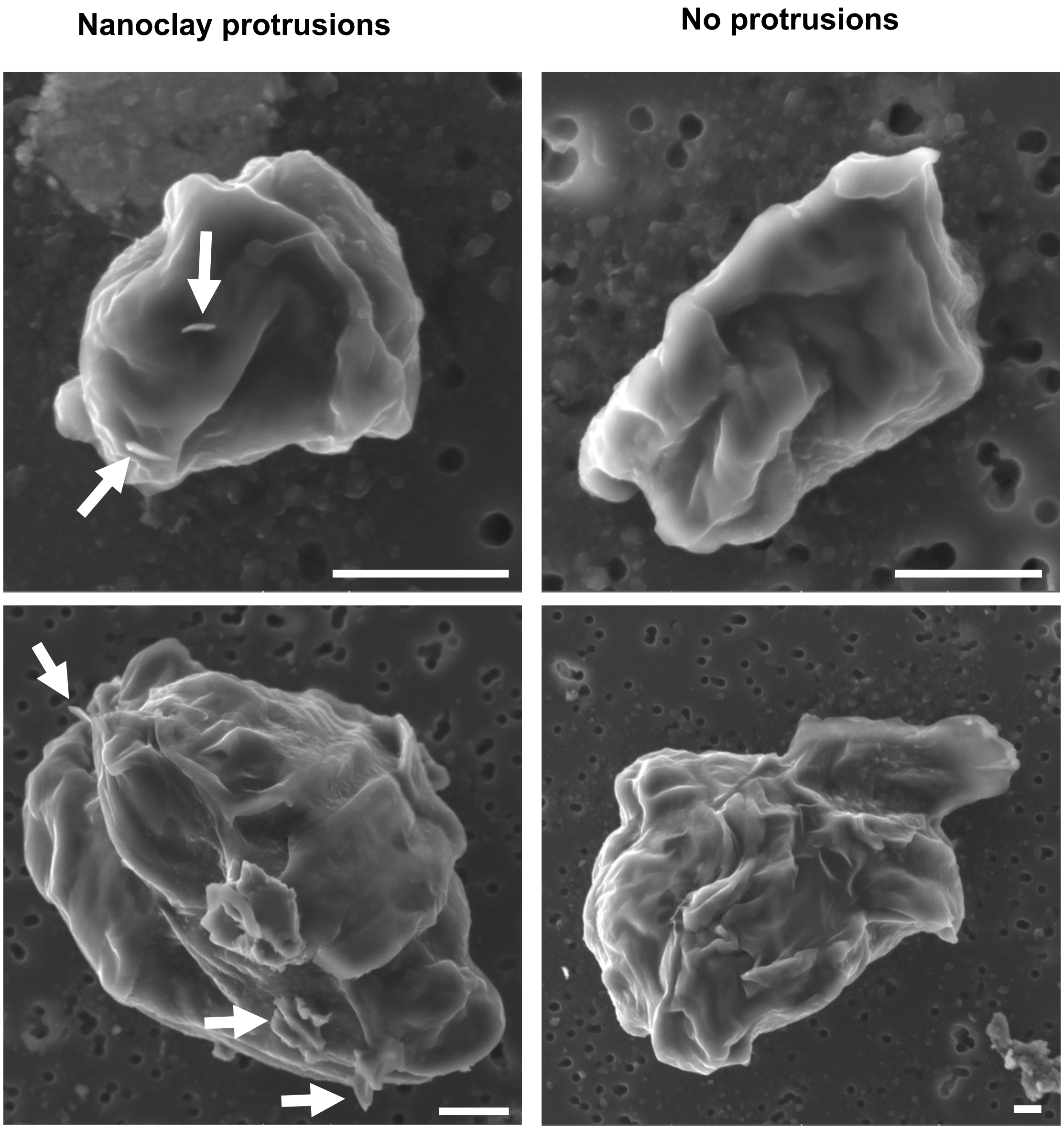

Nanoclay protrusions

No protrusions

Fig. S8. Representative diversity of 1% 93A PP nanocomposite particulate with (white arrows) and without nanoclay protrusions. Nanoclay protrusions were positively identified using manual FESEM/EDX spectra for both silica and aluminum presence. Scale bars represent 2 µm.